.

Organic-inorganic hybrid materials based on iron(III)-polyoxotungstates and 1-butyl-3-methylimidazolium cation

Filipe M. Santos, Paula Brandão, Vítor Félix, M. Rosário M. Domingues, João S. Amaral, Vítor S. Amaral, Helena I. S. Nogueira and Ana M. V. Cavaleiro

SUPLEMENTARY MATERIAL

Organic-inorganic hybrid materials based on iron(III)-polyoxotungstates and 1-butyl-3-methylimidazolium cation

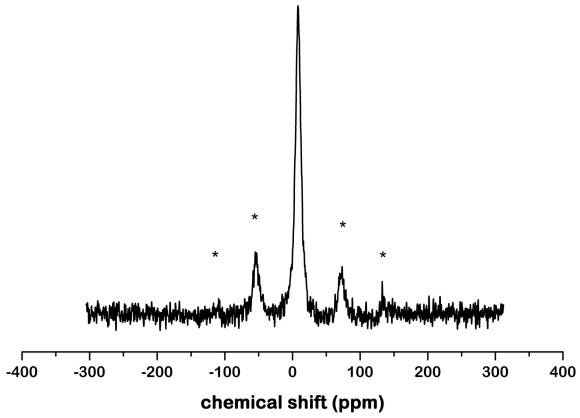

Figure S1. ^{31}P MAS NMR of $(Bmim)_{10}[(PW_{11}O_{39}Fe^{III})_2O]\cdot 0.5H_2O$ (**1**). (*) indicates sidebands.

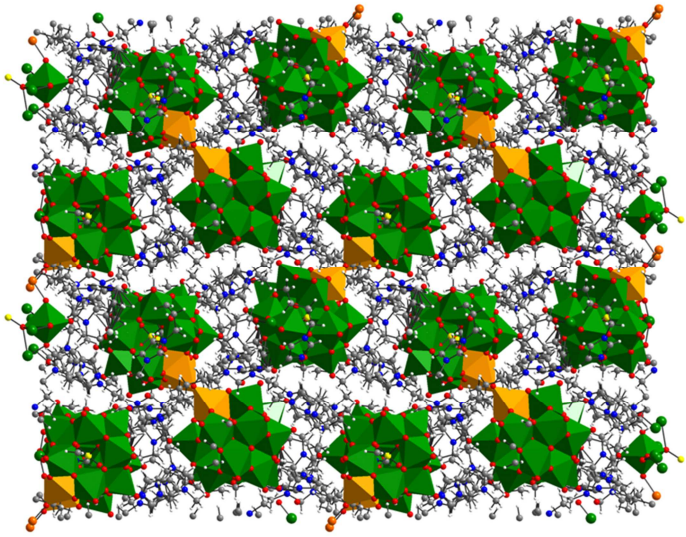

Figure S2. Crystal packing diagram of $(Bmim)_{10}[(PW_{11}O_{39}Fe)_2O]\cdot 0.5H_2O$ along the [001] crystallographic direction.

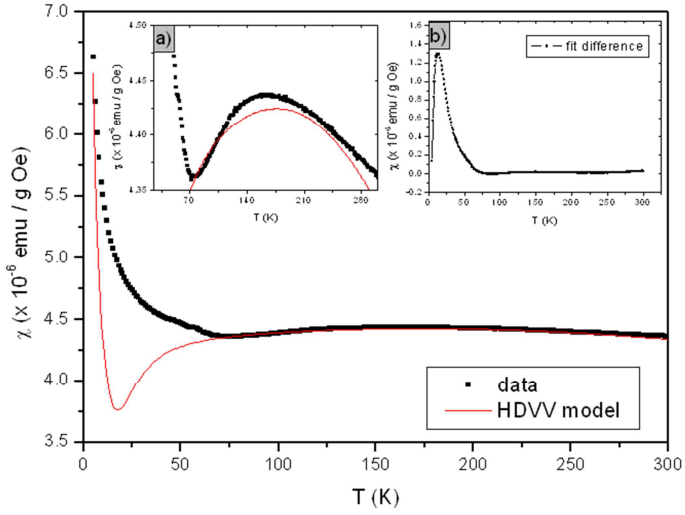

Figure S3 Magnetic susceptibility data and fit to the HDVV model (see text). Inset a) shows difference between data and preliminary analysis, and inset b) shows the detail of the susceptibility maximum at ~ 160 K.

Organic-inorganic hybrid materials based on iron(III)-polyoxotungstates and 1-butyl-3-methylimidazolium cation

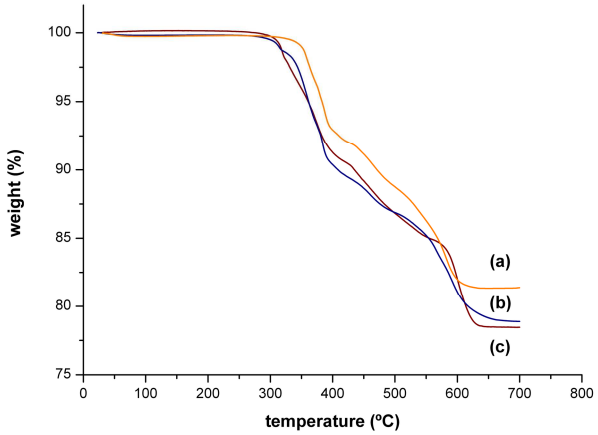

Figure S4 – Thermal gravimetric analyses of (a) $(Bmim)_4[PW_{11}O_{39}Fe^{III}(H_2O)]\cdot H_2O$ (**2**); (b) amorphous $(Bmim)_{10}[(PW_{11}O_{39}Fe^{III})_2O]\cdot 0.5H_2O$ (**1**) (c) crystallised $(Bmim)_{10}[(PW_{11}O_{39}Fe^{III})_2O]\cdot 0.5H_2O$ (**1**)

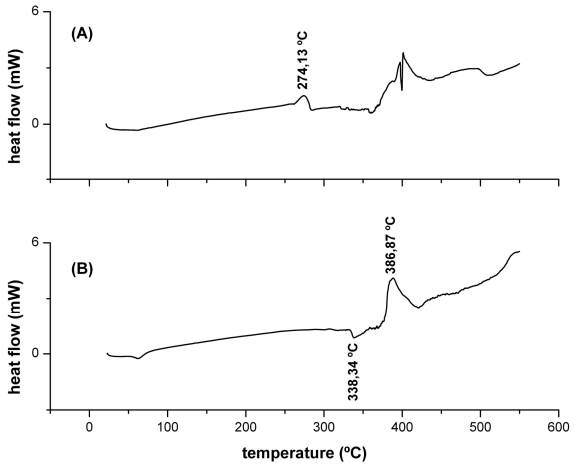

Figure S5. Differential scanning calorimetry measurements of (A) $(Bmim)_{10}[(PW_{11}O_{39}Fe^{III})_2O]\cdot 0.5H_2O$ (**1**) and (B) $(Bmim)_4[PW_{11}O_{39}Fe^{III}(H_2O)]\cdot H_2O$ (**2**).

Table S1. – MALDI-TOF MS data[(a)] (*m*/*z*) collected for $(Bmim)_{10}[(PW_{11}O_{39}Fe^{III})_2O]\cdot 0.5H_2O$ (**1**) and $(Bmim)_4[PW_{11}O_{39}Fe^{III}(H_2O)]\cdot H_2O$ (**2**)

α-cyano-4-hydroxycinnamic acid		Dithranol		Formula weight	Calculated values[(b)]	Species
(**1**)	(**2**)	(**1**)	(**2**)			
3271.1	3272.2	3272.3		3273.91	3274.7	$(Bmim)_4[PW_{11}O_{38}Fe^{II}]^+$
3428.4	3429.7	3429.3	3430.4	3429.13	3429.8	$(Bmim)_5[PW_{11}O_{39}Fe^{III}]^+$
		3492.9		3493.21	3493.8	$(Bmim)_5[PW_{11}O_{39}Fe^{III}](CH_4O)_2^+$
		3567.5	3568.4	3568.34	3568.9	$(Bmim)_6[PW_{11}O_{39}Fe^{II}]^+$
3601.5	3601.7			3601.29	3601.8	$(Bmim)_5[PW_{11}O_{38}Fe^{II}](C_{10}H_6NO_3^-)^+$
		3633.3		3632.43	3633.0	$(Bmim)_6[PW_{11}O_{39}Fe^{II}](CH_4O)_2^+$
6268.0	6267.0			6266.26	6266.9	$H_3KNa_2(Bmim)_5[(PW_{11}O_{39}Fe^{III})_2O]^{+(c)}$
6408.6	6410.5			6410.35	6411.0	$HNa_4(Bmim)_6[(PW_{11}O_{39}Fe^{III})_2O]^+$
6564.0	6562.0			6564.66	6565.1	$KNa_3(Bmim)_7[(PW_{11}O_{39}Fe^{III})_2O]^+$

(a) Values printed in spectra; (b) higher intensity ion in the isotopic pattern; (c) other possible ions may be considered.

Organic-inorganic hybrid materials based on iron(III)-polyoxotungstates and 1-butyl-3-methylimidazolium cation

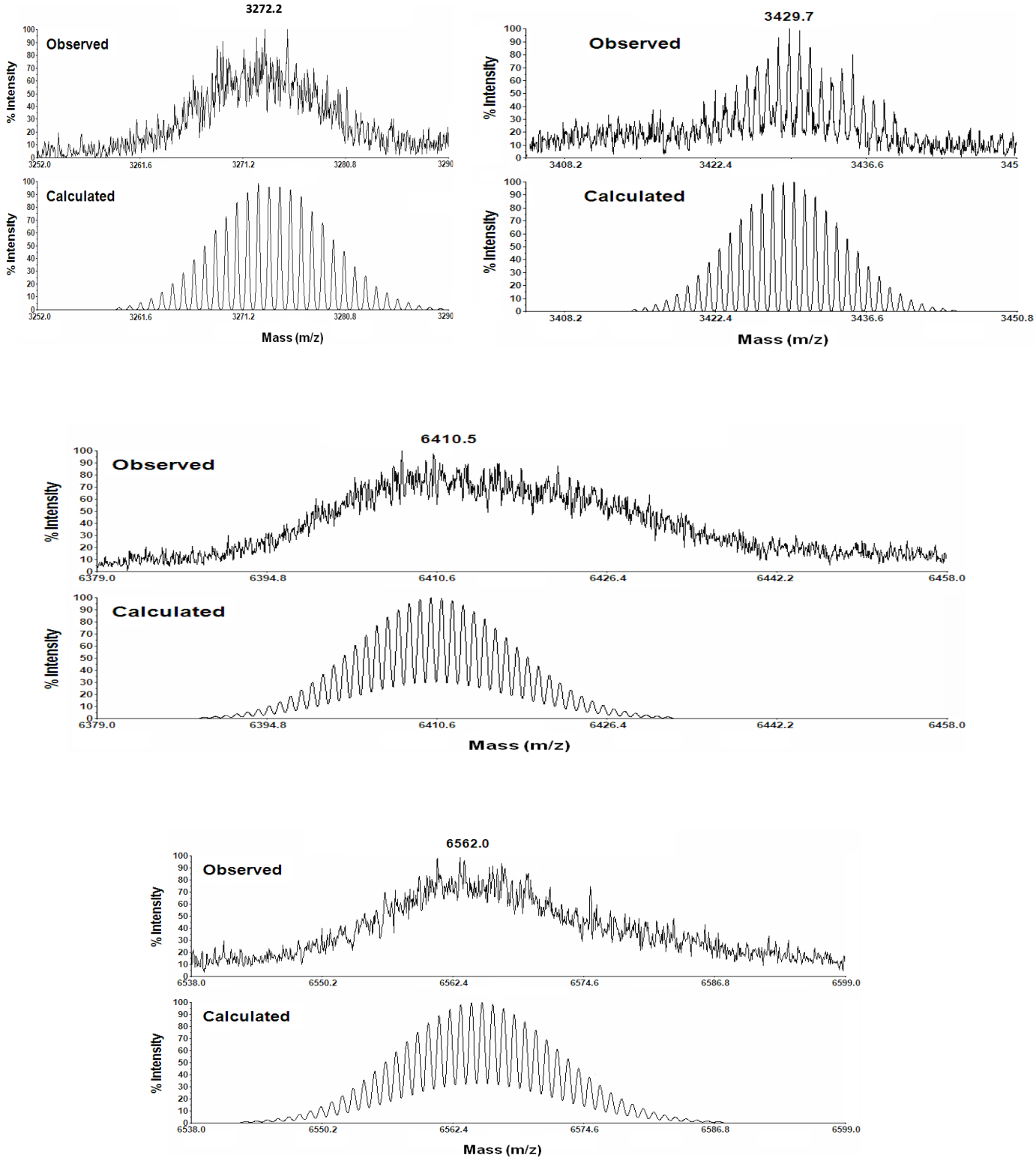

Figure S6. Experimental and simulates isotopic patterns of .MALDI-TOF MS (α-cyano-4-hydroxycinnamic acid matrix) of compounds **1** and **2** (see Table S1).

Organic-inorganic hybrid materials based on iron(III)-polyoxotungstates and 1-butyl-3-methylimidazolium cation

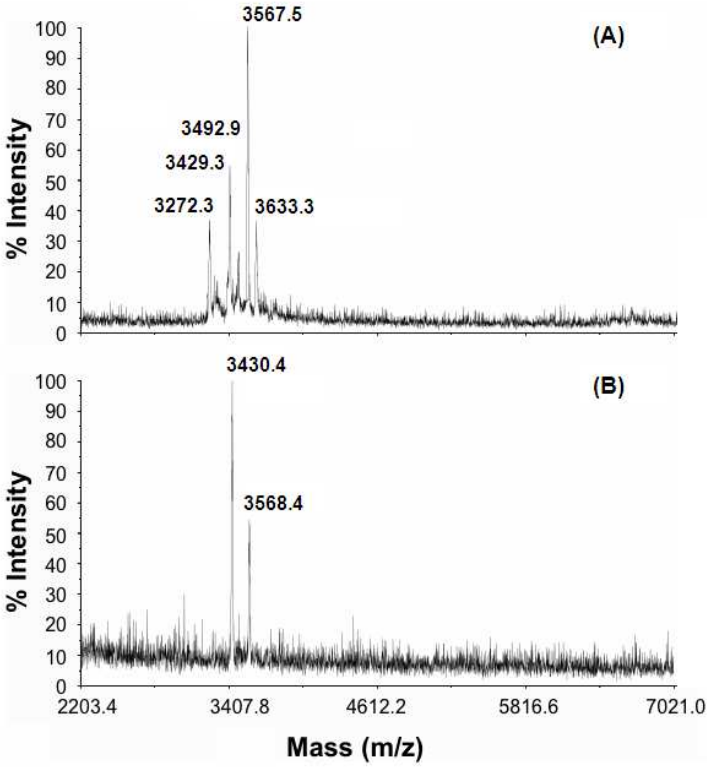

Figure S7. MALDI-TOF MS (dithranol matrix) of (A) $(Bmim)_{10}[(PW_{11}O_{39}Fe^{III})_2O]\cdot 0.5H_2O$ (**1**) and (B) $(Bmim)_4[PW_{11}O_{39}Fe^{III}(H_2O)]\cdot H_2O$ (**2**).

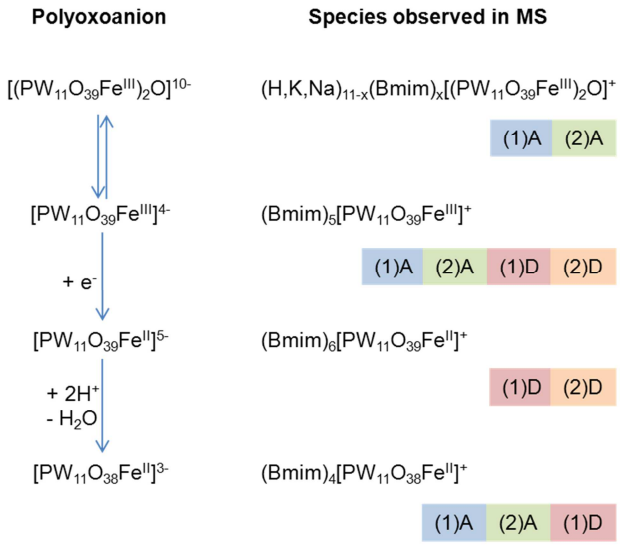

Scheme S1. Interrelations among the different polyoxoanions present in the most abundant species identified in the MALDI-TOF MS spectra. In boxes: (compound)/matrix, A = α-cyano-4-hydroxycinnamic acid, D = dithranol

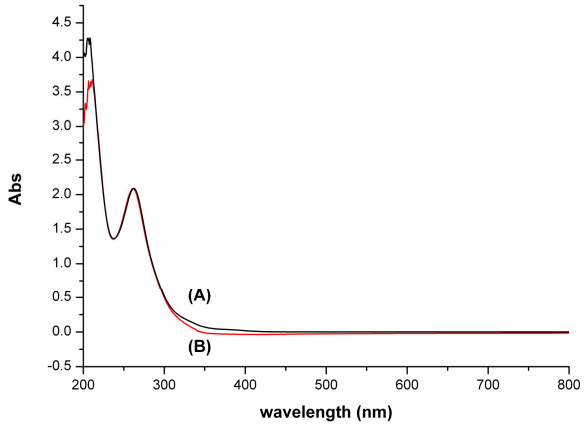

Figure S8 – Spectra of (A) compound **(2)** and (B) compound **(1)** in CH_3CN/H_2O (4:1) solutions; *C* (based on iron) = $5x10^{-5}$ M, b = 1 cm.

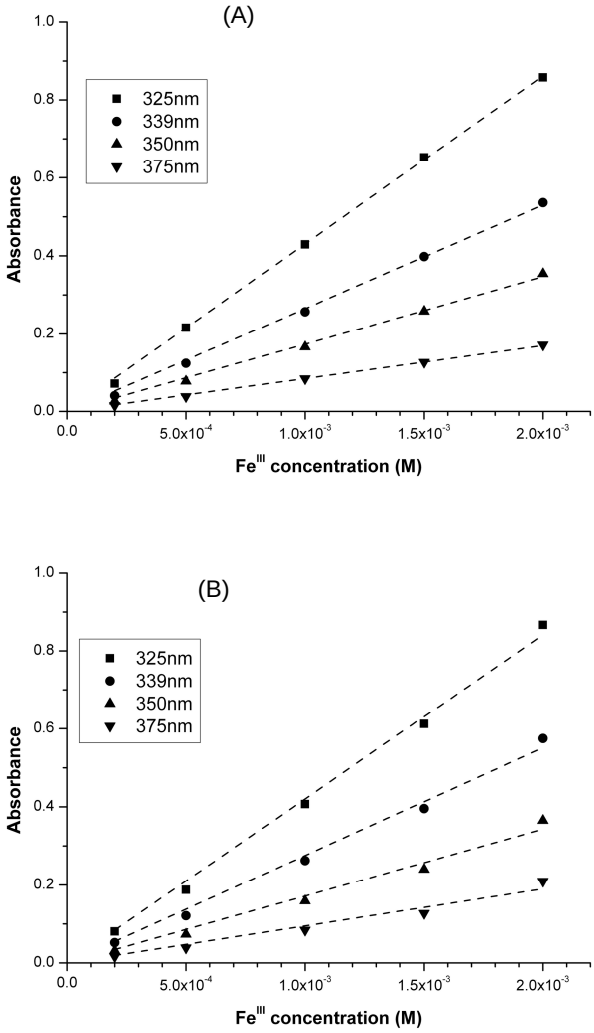

Figure S9. Variation of the absorbance, at various wavelengths, with the concentration (based on iron) of (A) compound **2**; (B) compound **1** acidified (1µL THF/mL) in CH_3CN/H_2O (4:1) solutions (b = 1 mm)

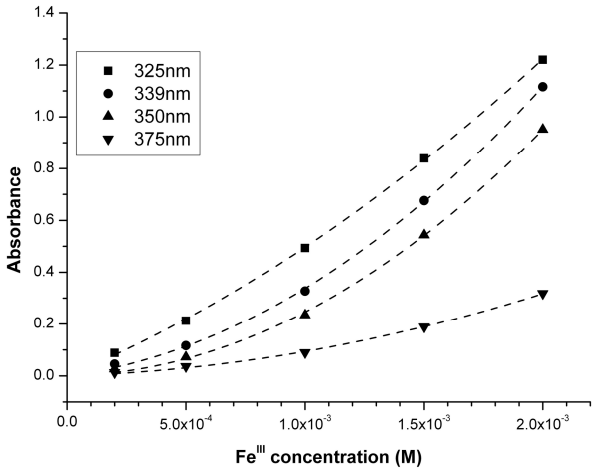

Figure S10. Variation of the absorbance, at various wavelengths, with the concentration (based on iron) of compound **1** in CH_3CN/H_2O (4:1) solutions (b = 1 mm)